The global phase diagram of the Gay–Berne model

Enrique de Miguel
Departamento de Física Aplicada, Escuela Politécnica Superior, Universidad de Huelva, 21819 La Rábida, Huelva, Spain

Carlos Vega
Departamento de Química Física, Facultad de Ciencias Químicas, Universidad Complutense de Madrid, 28040 Madrid, Spain

(Received 13 June 2002; accepted 11 July 2002)

The phase diagram of the Gay–Berne model with anisotropy parameters $\kappa=3$, $\kappa'=5$ has been evaluated by means of computer simulations. For a number of temperatures, *NPT* simulations were performed for the solid phase leading to the determination of the free energy of the solid at a reference density. Using the equation of state and free energies of the isotropic and nematic phases available in the existing literature the fluid–solid equilibrium was calculated for the temperatures selected. Taking these fluid–solid equilibrium results as the starting points, the fluid–solid equilibrium curve was determined for a wide range of temperatures using Gibbs–Duhem integration. At high temperatures the sequence of phases encountered on compression is isotropic to nematic, and then nematic to solid. For reduced temperatures below $T=0.85$ the sequence is from the isotropic phase directly to the solid state. In view of this we locate the isotropic–nematic–solid triple point at $T_{INS}=0.85$. The present results suggest that the high-density phase designated smectic B in previous simulations of the model is in fact a molecular solid and not a smectic liquid crystal. It seems that no thermodynamically stable smectic phase appears for the Gay–Berne model with the choice of parameters used in this work. We locate the vapor–isotropic liquid–solid triple point at a temperature $T_{VIS}=0.445$. Considering that the critical temperatures is $T_c=0.473$, the Gay–Berne model used in this work presents vapor–liquid separation over a rather narrow range of temperatures. It is suggested that the strong lateral attractive interactions present in the Gay–Berne model stabilizes the layers found in the solid phase. The large stability of the solid phase, particularly at low temperatures, would explain the unexpectedly small liquid range observed in the vapor–liquid region. © *2002 American Institute of Physics.* [DOI: 10.1063/1.1504430]

I. INTRODUCTION

Liquid crystals exhibit an unsually rich variety of phases with varying degree of positional and orientational order between the isotropic fluid and the crystalline phase.[1–3] The determination of the range of phase stability and characterization of their phase transitions is of major importance and have stimulated considerable theoretical and experimental research.[1–3] Considerable insight into general features of phase behavior in liquid crystals at a molecular level has been possible by the application of computer simulation in terms of molecular models.[4]

Models based on hard particles are of help in understanding the role of excluded volume interactions as the driving mechanism for phase transitions in liquid crystals, but obviously are not suitable for the study of thermotropic phase transitions. One of the most useful molecular models that incorporates explicitly anisotropy in both the attractive and repulsive interactions was long ago proposed by Gay and Berne.[5] The Gay–Berne (GB) model has become nowadays a standard model to the study of thermotropic liquid crystals.

In the GB model, molecules are considered as rigid units with axial symmetry. Each molecule i is represented by the position $\mathbf{r}_i$ of its center of mass, and a unit vector $\hat{\mathbf{u}}_i$ along its symmetry axis. The pair interaction between molecules i and j is given by

$$U_{ij}^{\mathrm{GB}}(\mathbf{r}_{ij},\hat{\mathbf{u}}_i,\hat{\mathbf{u}}_j)=4\epsilon(\hat{\mathbf{r}}_{ij},\hat{\mathbf{u}}_i,\hat{\mathbf{u}}_j)\times\left[\left(\frac{\sigma_0}{d(\mathbf{r}_{ij},\hat{\mathbf{u}}_i,\hat{\mathbf{u}}_j)}\right)^{12}-\left(\frac{\sigma_0}{d(\mathbf{r}_{ij},\hat{\mathbf{u}}_i,\hat{\mathbf{u}}_j)}\right)^{6}\right], \tag{1}$$

with $d(\mathbf{r}_{ij},\hat{\mathbf{u}}_i,\hat{\mathbf{u}}_j)=r_{ij}-\sigma(\hat{\mathbf{r}}_{ij},\hat{\mathbf{u}}_i,\hat{\mathbf{u}}_j)+\sigma_0$. Here σ_0 defines the smallest molecular diameter, r_{ij} is the distance between the centers of mass of molecules i and j, and $\hat{\mathbf{r}}_{ij}=\mathbf{r}_{ij}/\mathbf{r}_{ij}$ is a unit vector along the intermolecular vector $\mathbf{r}_{ij}=\mathbf{r}_i-\mathbf{r}_j$. The range σ and strength ϵ of the GB interactions depend on $\hat{\mathbf{u}}_i$, $\hat{\mathbf{u}}_j$, and $\hat{\mathbf{r}}_{ij}$. In addition, σ and ϵ depend on two anisotropy parameters, namely, the ratio of molecular length to breadth (κ), and the ratio of the potential well depths for the side-by-side and end-to-end configuration (κ'). The anisotropy of the well depth ϵ is also controlled by two additional parameters μ and ν. Explicit expressions for σ and ϵ may be found in the original paper by Gay and Berne.[5]

As it reads, the GB interactions define in fact a family of potential models each differing by the values chosen for the parameters κ, κ', μ, and ν. Note that for the particular choice $\kappa=\kappa'=1$, the GB potential reduces to the Lennard-Jones potential with $\sigma=\sigma_0$ and $\epsilon=\epsilon_0$. In their original work, Gay and Berne considered molecules with axial ratio $\kappa=3$, and the set of parameters $\kappa'=5$, $\mu=2$, $\nu=1$ in order

to mimic the anisotropic interactions in an equivalent linear-site Lennard-Jones potential. This parametrization has been widely used in computer simulation to study the phase behavior, liquid crystal properties,[6–12] and also in theoretical studies.[13,14] For this choice of parameters, the system exhibits phases identified as vapor (V), isotropic (I), and nematic (N), and the regions of stability have been determined by Gibbs ensemble simulation ($V-I$ region)[7,11] and thermodynamic integration ($I-N$ region).[8,12] At high density (or pressure) the GB system exhibits a layered phase identified as smectic B (SmB).[6,9,12] Simulations using different combinations of parameters have shown that the GB model exhibits an additional phase identified as smectic A (SmA).[15–18] All these simulation studies suggest that the occurrence of the SmB is not very sensitive to the particular parameterization, whereas the formation of the SmA phase requires the molecular elongation κ be large enough.

Despite all the effort devoted to understand the phase behavior of GB systems, there are still unresolved questions. For example, the relative thermodynamic stability of the different smectic phases with respect to the fluid (isotropic or nematic) phases has not been determined so far. Additionally, no systematic study of the GB solid phase has been reported and, consequently, whether or not the reported smectic phases are stable with respect to the solid remains an open question.

A further intriguing issue concerns the nature of the reported SmB phase for GB systems. In simple terms, the smectic phase can be viewed as a set of two-dimensional liquid layers stacked on each other with a well-defined interlayer spacing.[2] The simplest (orthogonal) smectic phase is the smectic A (SmA) in which there is no in-plane positional correlations. In the SmB phase, each smectic layer is again a two-dimensional liquid but the in-plane structure is markedly different from that of the SmA. In the SmB phase, the centers of mass are hexagonally distributed in each layer, these hexagons being everywhere parallel to one another (this phase is also named hexatic B,[19] hexatic smectic[2] or simply hexatic phase; according to Goodby and Gray,[19] the recommended nomenclature for this phase in SmB). This type of order is referred to as (sixfold) bond orientational order (BOO).[1,2,20,21] Long-range BOO is also exhibited by three dimensional crystals, although crystalline phases also display three-dimensional long-range positional order, in contrast to the short-range intralayer positional order of the SmB phase. Birgenau and Lister[22] were the first to suggest the existence of the SmB phase, carrying over to liquid crystals in three dimensions the concepts introduced by Halperin and Nelson[23] on two-dimensional melting. Hexatic order in liquid crystals was later observed unambiguously by Pindak *et al.*[24] Careful high-resolution x-ray diffraction experiments and the use of freely suspended films[25] showed that most of the phases previously labeled as SmB did not have hexatic order but were crystalline phases. This crystal phase has been typically referred to as crystalline smectic B or crystal B phase (the former terminology is, however, misleading as the phase is not a true smectic liquid crystal). The crystal B phase has been shown to exhibit unusual features (not shared by conventional molecular crystals), such as the ability of suffering plastic deformations under weak external forces, or a sequence of restacking transitions (involving significant shifts in the relative position of the molecular centers of mass of adjacent layers) as the temperature is lowered. These facts show that this phase must be characterized by an unusually weak coupling between layers.

In principle, the strong (attractive) side-by-side molecular interactions of the GB model are expected to promote the formation of smectic phases. This seemed to be confirmed by the simulations of Luckhurst *et al.*[6] and de Miguel *et al.*,[9] in which there were clear indications that GB systems developed layered structures at high density (at a given temperature) or at low temperature (at a given density) with a nearly hexagonal distribution of the molecular centers of mass within the layers. Although identified as SmB, whether it was smecticlike or crystalline was recognized as a subtle problem. As noted by Allen *et al.*,[16] on cooling the SmB phase to very low temperatures no transition to a crystal could be identified and the SmB exhibited well-defined correlations characteristic of crystalline packing. Further evidence of the crystalline nature of the SmB phase was obtained after the calculation of the shear elastic modulus by Brown *et al.*[17] On the basis of all this evidence, it was suggested that the reported SmB phase for the GB model was in fact crystalline and that it might be more appropriate to refer to this phase as a solid.

The work reported here concentrates on the solid phase for GB systems with the original set of parameters, as well as on the location of the corresponding fluid–solid transition. A description of the simulation techniques and methodology is given in Sec. II. The simulation results are presented and discussed in Sec. III, and the resulting temperature–density and pressure–temperature phase diagrams of the GB system are presented in Sec. IV.

II. SIMULATION METHODOLOGY

In order to be consistent with previous simulations of the model, the GB intermolecular potential was truncated at a distance $r_c=4\sigma_0$ and shifted such that $U(r_{ij}=r_c)=0$. All quantities are expressed in conventional reduced units, using σ_0 and ϵ_0 as units of length and energy, respectively. The orientational order was characterized by the second-rank order parameter S, defined as the largest eigenvalue of the order tensor.[26] The eigenvector associated to S was identified as the director of the orientationally ordered phase.

To probe the in-layer structure, we have calculated the two-dimensional in-plane positional correlation function $g_\perp(r_\perp)$, where $r_\perp$ is the the distance between a pair of particles (belonging to the same layer) perpendicular to the director of the phase. This function is expected to be liquidlike (short-range in-plane positional correlations) for any smectic phase and to show considerable structure (long-range in-plane positional correlations) for the solid phase, thereby allowing to distinguish the SmB from the crystal phase.

For the location of the fluid–solid transition we have calculated the free energy of the fluid (isotropic or nematic) and solid phases by thermodynamic integration along four isotherms, namely $T=1.25$, 0.95, 075, and 0.50. Details of these calculations are given in the sections below. The coex-

istence points are subsequently obtained by imposing equality of pressure and chemical potential of both phases and they are used as starting points to obtain the complete melting curve by Gibbs–Duhem (GD) integration.

A. Free energy of the fluid phases

The computation of the free energy of the fluid phases along an isotherm requires prior knowledge of the corresponding EOS. For the lowest temperature considered in this work ($T=0.50$), the EOS for the (isotropic) fluid phase was obtained by performing standard constant NVT MC simulations, where N is the number of particles, V is the volume, and T is the temperature. We recall that at this temperature the only expected fluid phase is isotropic.

We considered systems of $N=500$ molecules in a cubic box. At low densities, the molecules were placed on the sites of a fcc lattice, and the system was allowed to melt into the fluid phase. The system was then brought to higher densities by slowly compressing the fluid phase in small increments of density. At each density, the pressure was sampled over 100 000 cycles after an initial equilibration stage of 100 000 cycles. The Helmholtz free energy at any (fluid) density along the isotherm $T=0.50$ was calculated by thermodynamic integration according to the following expression:

$$\frac{F(\rho)}{Nk_BT}=\frac{F_{\mathrm{id}}(\rho)}{Nk_BT}+\int_0^{\rho}d\rho'\frac{P(\rho')}{\rho'^2k_BT}, \tag{2}$$

where $\rho=N/V$ is the number density, P is the pressure, $F_{\mathrm{id}}/(Nk_BT)=\ln\rho-1$ is the free energy of the ideal gas at density ρ and k_B is Boltzmann's constant.

According to previous investigations,[12] in addition to the isotropic phase, the GB fluid exhibits nematic behavior along the isotherms $T=0.75$, 0.95, and 1.25. The free energies of both the isotropic and nematic phases were already computed in Ref. 12 to locate the $I-N$ transition, and they have been used here to locate the corresponding fluid–solid transition. For the present calculations, we did not include the temperature-dependent term $(-5/2\ln T)$ in the free energy of the ideal gas considered in Ref. 12. Obviously, this will only shift the absolute values of the free energy (or the chemical potential) but will not affect the transition properties.

B. Simulation of the solid phase

All simulations of the solid phase presented in this work were performed in the NPT ensemble. In particular we used the Monte Carlo (MC) scheme developed by Yashonath and Rao[27] in which volume fluctuations are performed by allowing for arbitrary changes in the shape of the simulation box. This is important when simulating solids since it avoids any possible metastability resulting from the constraint of fixing the shape of the simulation cell. This method can be regarded as the MC version of the molecular dynamics method devised by Parrinello and Rahman.[28] Volume fluctuations were performed by sampling the elements of the h matrix, where h is the 3×3 matrix that relates the real ($\mathbf{r_i}$) and the scaled ($\mathbf{s_i}$) coordinates of the molecular centers of mass, i.e., $\mathbf{r_i}=h\mathbf{s_i}$.[27,28] Note that $h=\{\mathbf{a},\mathbf{b},\mathbf{c}\}$, where the vectors $\mathbf{a}$, $\mathbf{b}$, and $\mathbf{c}$ define the edges of the simulation box.

One important issue when simulating solids is the choice of the initial solid structure. As it happens with most molecular models, the equilibrium crystal structure of the GB model is not known *a priori*. In principle, one should propose several solid structures and consider their *relative* thermodynamic stability by evaluating their free energy differences (which, on the other hand, are expected to be very small). However, this procedure does not give information on which is the true equilibrium structure. Further, it may well happen that the thermodynamically stable structure be different at different temperatures.

In the present work, we did not address the question of the relative stability among different structures and decided to start from a sensible choice for the initial solid structure. In particular, we considered layers with hexagonal arrangement of the molecular centers. These layers are stacked following an *ABC* sequence configuration analogous to the fcc lattice and stretched along the $\mathbf{c}$ axis. The layers were placed parallel to the $\mathbf{a}-\mathbf{b}$ plane and the molecules were initially oriented perpendicular to the layers. We considered six layers, each layer consisting of 9×9 molecules. Thus, this arrangement yields a total number of $N=486$ molecules. In some cases, we also considered significantly larger systems of $N=3150$ molecules arranged in six layers (*ABC* stacking) with 21×25 molecules in each layer.

The simulations were organized in MC cycles, each cycle consisting of N attempts to displace or rotate the molecules and one attempt to change the volume and the shape of the simulation cell. For each temperature, the solid branch of the isotherm was obtained starting from a crystal structure at high pressure. Subsequently, the system was expanded by slowly decreasing the input pressure. In all cases, the initial configuration was taken from the final configuration of the previous (higher) pressure. At each input pressure, the system was typically equilibrated for 100 000 cycles and thermodynamic averages were collected over 100 000 additional cycles.

Typically, 10–15 (solid) state points were simulated for each of the isotherms ($T=1.25$, 0.95, 0.75, and 0.50) considered in this work. Thermodynamic results for several selected state points on the solid phase are presented in Table I.

C. Free energy of the solid phase

Once the EOS for the solid phase is known free energy calculations for the solid phase should be performed in order to locate the melting transition. To this purpose, we used the Frenkel–Ladd method[29] as extended to nonspherical particles by Frenkel and Mulder.[30,31] In this method, the free energy of the solid is related to that of an ideal classical Einstein crystal of the same structure. In the ideal Einstein crystal there is no intermolecular interactions, and each molecule of the system is constrained to the original lattice configuration by a harmonic potential U_i of the form

$$U_i=\lambda_1(\mathbf{r}_i-\mathbf{r}_i^0)^2+\lambda_2\sin^2\alpha_i, \tag{3}$$

where $\mathbf{r}_i$ is the current position of particle i, $\mathbf{r}_i^0$ its lattice equilibrium position and α_i is the angle between the axis of molecule i and the axis of the same molecule in the equilib-

TABLE I. Thermodynamic properties of the GB model in the solid phase as obtained from *NPT* MC simulations at different temperatures T and pressures P. ρ is the number density, U is the configurational energy per particle, H is the enthalpy per particle, and S is the orientational order parameter. Results are for systems of $N=486$ molecules, except for those marked with a † which correspond to systems of $N=3150$ molecules.

T	P	ρ	U	H	S
1.25	13.0	0.4035(4)	−3.61(2)	31.73(5)	0.964(2)
1.25	11.0	0.3935(5)	−3.84(3)	27.24(6)	0.957(2)
1.25	9.0	0.3816(4)	−4.02(3)	22.69(4)	0.949(2)
1.25	8.0	0.3742(7)	−4.07(4)	20.44(7)	0.942(3)
0.95	12.0	0.4082(3)	−4.19(2)	27.58(3)	0.976(1)
0.95†	12.0	0.4085(2)	−4.18(1)	27.57(2)	0.976(1)
0.95	9.0	0.3934(4)	−4.54(2)	20.71(4)	0.969(1)
0.95†	9.0	0.3936(2)	−4.55(1)	20.70(2)	0.970(1)
0.95	7.0	0.3803(5)	−4.71(2)	16.07(4)	0.963(2)
0.95†	7.0	0.3806(2)	−4.71(1)	16.06(2)	0.963(1)
0.95	5.0	0.3625(7)	−4.74(4)	11.43(6)	0.951(3)
0.95†	5.0	0.3628(2)	−4.74(1)	11.42(1)	0.951(1)
0.75	7.0	0.3893(4)	−5.08(1)	14.78(3)	0.976(1)
0.75	5.0	0.3742(4)	−5.19(2)	10.05(3)	0.969(1)
0.75	3.0	0.3513(6)	−5.12(2)	5.30(3)	0.955(2)
0.75	2.0	0.3328(8)	−4.90(3)	2.98(4)	0.939(3)
0.50	4.0	0.3794(3)	−5.74(8)	6.05(1)	0.982(1)
0.50	2.0	0.3572(3)	−5.70(1)	1.15(2)	0.974(1)
0.50	0.5	0.3222(10)	−5.26(2)	−2.46(3)	0.953(2)
0.50	0.3	0.3127(9)	−5.10(2)	−2.89(3)	0.955(2)

rium lattice. In Eq. (3), λ_1 and λ_2 are coupling constants. We refer the reader to the paper of Frenkel and Mulder[30] and to the work of Vega *et al.*[32] for further details. The final expression for the Helmholtz free energy of the GB solid at a given density may be expressed as

$$F=F_E+\Delta F_1+\Delta F_2+\Delta F_3, \tag{4}$$

where F_E is the free energy of the ideal Einstein crystal, ΔF_1 is the difference between the free energy of the ideal Einstein crystal and that of the Einstein crystal with GB intermolecular interactions, ΔF_2 is the difference between the free energy of the GB solid and that of the Einstein crystal with GB interactions, and ΔF_3 is the difference in free energy between a system of unconstrained center of mass and one of fixed center of mass. We refer the reader to the Refs. 29–32 for further details. The Frenkel–Ladd method has become the standard way of getting the free energy of solids, although certainly there are other alternatives.[33]

For each temperature, we have evaluated the free energy of the solid phase at a certain (solid) density. At $T=0.95$, two different densities within the solid branch were considered. The free energy calculations were performed at fixed density using the equilibrium simulation box shape obtained from the *NPT* simulations.

Once the free energy at a certain density ρ_1 is known, the free energy at any other density ρ_2 within the isotherm follows from thermodynamic integration using the expression:

$$\frac{F}{Nk_BT}(\rho_2,T)=\frac{F}{Nk_BT}(\rho_1,T)+\int_{\rho_1}^{\rho_2}\frac{P(\rho,T)}{\rho^2k_BT}d\rho. \tag{5}$$

TABLE II. Free energy values $F_{\mathrm{ref}}/(Nk_BT)$ for GB systems in the solid phase at the reference density ρ and temperature T.

State	T	ρ	$F_{\mathrm{ref}}/(Nk_BT)$
1	1.25	0.383 49	4.889
2	0.95	0.354 05	2.469
3	0.95	0.384 10	3.798
4	0.75	0.359 44	1.283
5	0.50	0.384 86	−1.170

In the same way, if the free energy at a certain temperature T_1 is known, the free energy at any other temperature T_2 within the isochore can be obtained from the relation

$$\frac{F}{Nk_BT}(\rho,T_2)=\frac{F}{Nk_BT}(\rho,T_1)-\int_{T_1}^{T_2}\frac{U(\rho,T)}{Nk_BT^2}dT, \tag{6}$$

where U is the internal potential energy.

All free energy calculations for the solid phase were performed for systems of $N=486$ molecules, and with runs of about 100 000 cycles for equilibration and 100 000 cycles for thermodynamic averages. The maximum value used for the harmonic (positional) spring λ_1 of the Einstein crystal was 10 000 (in units of k_BT/σ_0^2) and 10 000 (in k_BT units) for the orientational spring λ_2. In Table II the free energies of the solid phase for the considered states are shown.

A good consistency test is to check how the free energy difference between two selected states obtained according to the above prescriptions compares with that obtained from thermodynamic integration. We considered four different pairs of states and found fully consistent results. We estimate the uncertainty of our free energy calculation for a certain state to be about 0.02 (in Nk_BT units).

D. Gibbs–Duhem integration

An accurate location of the fluid–solid transition by thermodynamic integration at a given temperature would involve a significant investment of computing time. In order to trace out the fluid–solid phase boundaries in thermodynamic space we made use of the Gibbs–Duhem (GD) integration method developed by Kofke.[34–36] In its simplest version, the GD method involves integration of the Claussius–Clapeyron equation,

$$\left(\frac{dP}{dT}\right)_{FS}=\frac{\Delta h}{T\Delta v}, \tag{7}$$

where $\Delta h=h_F-h_S$ and $\Delta v=v_F-v_S$ are the differences in enthalpy and volume per particle of the fluid (F) and solid (S) phases, respectively. Equation (7) is a first-order differential equation representing the change in coexistence pressure in terms of temperature along the melting curve. In practice, it is more convenient to cast Eq. (7) in a slightly different form,

$$\left(\frac{d\ln P}{d\beta}\right)_{FS}=-\frac{T\Delta h}{P\Delta v}\equiv\Phi(P,T), \tag{8}$$

where β is the inverse temperature. Integration in Eq. (8) can be performed provided the coexistence properties are known

at a given starting (initial condition) temperature T_0. For the present purposes, we use as starting points for implementing the GD scheme the coexistence points on the melting curve previously located by free energy calculations.

In practice, two systems, representing the coexisting fluid and solid phases are simultaneously simulated at constant P and T, with P being the corresponding fluid–solid coexistence pressure at the input temperature T, and the value of Φ is evaluated. Following a predictor–corrector scheme, a coexistence pressure $P_p(T')$ is predicted at a new temperature T' according to the Euler–Cauchy algorithm[37]

$$P_p(T') = P(T)\exp[\Phi(P,T)\Delta\beta], \tag{9}$$

where $\Delta\beta = \beta' - \beta$. Next, both systems are simulated at constant pressure and temperature T'; the run is divided into n_b blocks (each block consisting of 5000 MC cycles) and the pressure is corrected every block. Each block is run at constant pressure $P_n(T')$ $(n=1,2,...,n_b)$, with $P_1(T') = P_p(T')$. The value of the corrected pressure over successive blocks is obtained from the general Adams–Moulton corrector of second order[37] (trapezoidal rule) and is given by

$$P_{n+1}(T') = P(T)\exp\{\tfrac{1}{2}[\Phi_n(T') + \Phi(T)]\Delta\beta\}, \tag{10}$$

where $\Phi_n(T')$ is the average of Φ over block n. The coexistence pressure at temperature T' is finally obtained as the mean value of the block averages,

$$P(T') = \frac{1}{n_b}\sum_{n=1}^{n_b} P_j(T'). \tag{11}$$

A production run at this pressure provides the value of Φ at T' and the whole process is repeated for the next temperature.

We note that, although a general predictor–corrector algorithm is a multistep method (i.e., the solution at a given point depends on the solution at several previous points), the scheme implemented here (first order for the predictor step and second order for the corrector step) is, in fact, a single-step method: the solution of the differential equation (pressure) at a given temperature depends *only* on the solution at the previous temperature. Thus, the integration step size need not be fixed along the simulation series.

The GD scheme was applied to determine the fluid–solid coexistence curve for temperatures $T<1.25$. MC simulations in the *NPT* ensemble were performed in each phase simultaneously considering 500 molecules in the fluid phase and 486 molecules in the solid phase. The simulations were organized in cycles, each cycle consisting of trial displacements or rotations of all the molecules and one attempt to change the volume of each phase.

For the solid phase, we used the Yashonath and Rao MC scheme previously discussed. For the fluid phase, the pressure was kept fixed by performing trial isotropic volume fluctuations and therefore the box shape (initially cubic) remained unaltered during the simulation. At the initial starting temperature, T_0, the initial configuration of the fluid and solid phases were taken from final configurations of state points sufficiently close to the transition pressure. Both subsystems were then equilibrated at the transition pressure for 150 000 MC cycles and averages were taken over 150 000 additional MC cycles. Among others, we followed the behavior of quantities such as the number density ρ, configurational energy per particle U, enthalphy per particle h, nematic order parameter S, and the right-hand side of the Claussius–Clapeyron equation, Φ.

TABLE III. Details of the different series of GD integrations performed in the present work to study the fluid–solid coexistence of the GB model. The second column indicates the temperature on the coexistence line used to start the GD integration in the corresponding temperature range (third column). The last column indicates the nature of the fluid phase (isotropic or nematic) in coexistence with the solid phase in each series.

Series	Starting T	Temperature range	Integration direction	Observed $F-S$ coexistence
1	1.25	$1.25>T\geqslant 0.95$	Cooling	$N-S$
2	0.95	$0.95>T\geqslant 0.75$	Cooling	$N-S$ and $I-S$
3	0.75	$0.75<T\leqslant 0.95$	Heating	$I-S$ and $N-S$
4	0.75	$0.75>T\geqslant 0.50$	Cooling	$I-S$
5	0.50	$T<0.50$	Cooling	$I-S$

From this starting point, a GD integration series was initiated either increasing or decreasing the temperature in small increments ΔT (typically, $\Delta T = 0.001-0.020$ with the smallest value for the lowest temperatures) and the pressure was predicted according to Eq. (9). The fluid and solid phases were allowed to accommodate to the new (predicted) pressure value for 50 000 MC cycles and afterwards, the pressure was corrected over 150 000 additional MC cycles. This corrector stage was divided in $n_b = 30$ blocks (each block consisting of 5000 MC cycles) and the coexistence pressure was evaluated according to Eq. (11). Coexistence data were finally obtained as averages over 150 000 additional MC cycles. A summary of the main details of the GD integrations is given in Table III.

III. RESULTS AND DISCUSSION

The highest temperature investigated in this work was $T=1.25$. As reported in Ref. 12, on compressing the isotropic phase at this temperature, the GB fluid undergoes a transition to a nematic phase. Based on free energy calculations, the $I-N$ transition has been shown to take place at $P_{IN} = 5.20$.[12] The corresponding solid branch of the isotherm was obtained expanding a solid configuration at high pressure ($P=13.0$). The solid phase was found to be mechanically stable up to $P=5.5$. Below this pressure, the solid melted into the nematic phase. Results for some solid state points at $T=1.25$ have been included in Table I. The free energy of the solid phase was computed according to the procedure described in the previous section. By solving the equilibrium conditions, the $N-S$ transition was found to take place at $P_{NS}=7.68$. The behavior of the GB fluid along the isotherm $T=1.25$ is shown in Fig. 1.

At the next temperature considered here ($T=0.95$) the $I-N$ nematic transition was located at $P_{IN}=3.31$ from free energy calculations. As reported by de Miguel,[12] the nematic phase is mechanically stable upon compression up to $P=4.90$. Beyond this pressure, the nematic phase transforms (very slowly) into a higher density phase with a high degree

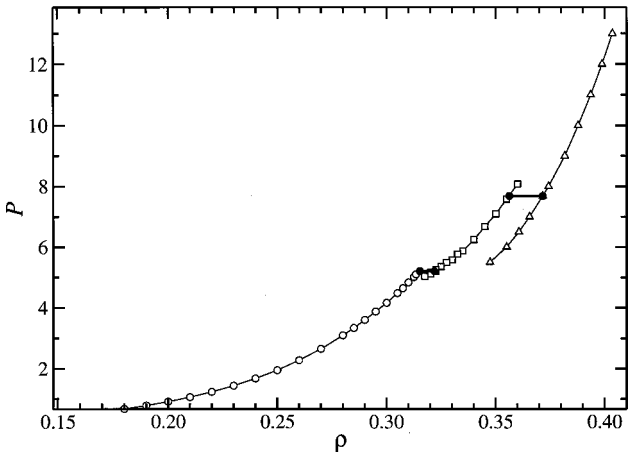

FIG. 1. Equation of state, showing isotropic (open circles), nematic (open squares), and solid (open triangles) phases, for the GB model at temperature $T=1.25$. The isotropic and nematic data are taken from Ref. 12 and the solid data are obtained from constant pressure MC. Filled symbols indicate the location of the isotropic-to-nematic and nematic-to-solid transition densities.

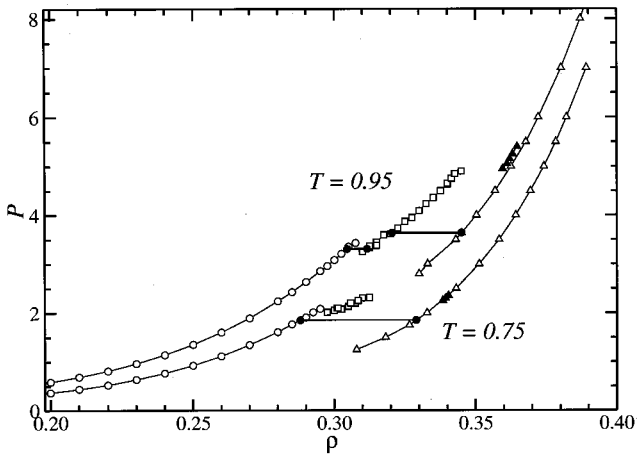

FIG. 2. Equation of state of the GB model at temperatures $T=0.95$ (upper curve) and $T=0.75$ (lower curve) showing isotropic (open circles), nematic (open squares) and solid (open triangles) phases. The isotropic and nematic data are taken from Ref. 12 and the solid data are obtained from constant pressure MC. Filled triangles correspond to simulation data for the SmB phase reported in Ref. 12. At $T=0.95$, the $I-N$ transition is followed by a $N-S$ transition at higher pressure. At $T=0.75$, the $I-N$ transition is pre-empted by the $I-S$ transition. Filled circles indicate the location of the different transitions.

of translational order. Although with some caveats, this phase was considered to be a SmB. We shall come to this point later.

The simulation of the solid phase at $T=0.95$ was started at $P=13.0$. The solid was subsequently expanded up to $P=2.5$. At this pressure, the solid melted *directly* into an isotropic fluid: no nematic behavior was found upon expanding the solid phase. Nonetheless, after calculating the free energy of the solid phase, and using the free energy of the nematic and isotropic phases, it was found that the solid–nematic transition takes place *before* the solid melts into the isotropic fluid. According to our calculations, it follows that $P_{NS}=3.64$. Thus, the nematic phase is thermodynamically stable at this temperature, although over a narrow range of pressures (or densities). Figure 2 shows the behavior of the GB fluid at $T=0.95$. The simulation results for the SmB phase reported by de Miguel[12] have been included in Fig. 2 for comparison. As can be seen in the figure, the differences between the solid and the SmB densities at a given pressure are small, and we believe that these SmB states correspond, in fact, to quasicrystalline (or imperfect solid) structures resulting from compressing the (nematic) fluid.

At temperature $T=0.75$ the $I-N$ transition was located at $P_{IN}=2.06$ from free energy calculations[12] and the nematic phase was found to be mechanically stable up to $P=2.20$. At this pressure, the nematic phase is driven upon compression to a layered phase identified as SmB in Ref. 12. The solid phase at $T=0.75$ was simulated starting from $P=7.0$ The resulting equilibrated configuration was slowly expanded in small pressure steps up to $P=1.25$. Below this pressure, the solid phase melted into the isotropic phase. As observed for $T=0.95$, no intermediate nematic phase was formed on expanding the solid phase. Interesting enough, the $I-N$ transition is pre-empted at this temperature by freezing, which occurs, according to the free energy calculations of the present work, at $P_{IS}=1.85$. Hence, for $T=0.75$, the nematic phase is not thermodynamically stable. The simulation results for the GB fluid at $T=0.75$ are shown in Fig. 2. Also shown in the figure are the results for the SmB phase in the compression runs reported by de Miguel,[12] the resulting densities falling on top of the solid branch of the isotherm. This gives further evidence to the fact that the reported SmB phase seems to correspond to a crystal structure.

Simulation results for $T=0.50$ are presented in Fig. 3. The (isotropic) fluid branch of the isotherm was obtained by compressing a low-density fluid in small increments of density up to a maximum value $\rho=0.260$. The solid phase was obtained by expanding a solid configuration starting at $P=5.0$ up to $P=1.0$. Below this pressure, the solid melted into an isotropic fluid. No nematic phase was observed. The free energies of the isotropic and solid phases were computed from thermodynamic integration and the transition was found to occur at $P_{IS}=0.24$ after solving the equilibrium conditions.

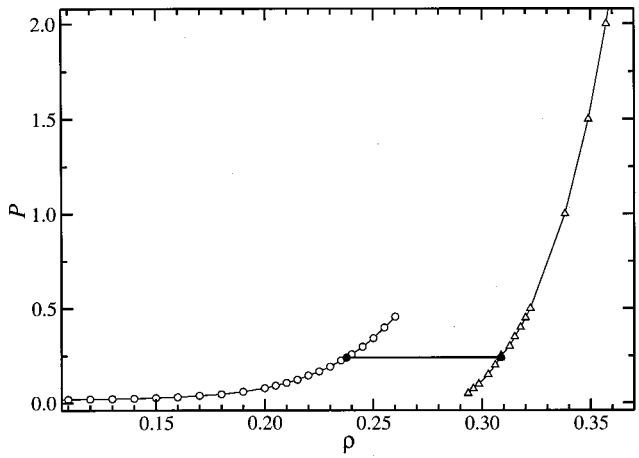

FIG. 3. Equation of state of the GB model at temperature $T=0.50$ showing isotropic (open circles) and solid (open triangles) phases. Filled circles indicate the location of the $I-S$ transition densities.

TABLE IV. Thermodynamic properties at the fluid–solid transition for the GB model as obtained from free energy calculations (†) at various temperatures. T for comparison, results obtained from Gibbs–Duhem integration at the end of the cooling (‡) and heating series (§) are also included. ρ_F and ρ_S are the fluid (isotropic or nematic) and solid number densities, respectively, and P_{FS} is the transition pressure.

T	Transition	ρ_F	ρ_S	P_{FS}
$1.25^{\dagger}$	$N-S$	0.3562(9)	0.3715(6)	7.68
$0.95^{\dagger}$	$N-S$	0.3205(12)	0.3450(8)	3.64
$0.95^{\ddagger}$	$N-S$	0.3223(13)	0.3467(9)	3.739(1)
$0.95^{\S}$	$N-S$	0.3203(15)	0.3454(8)	3.669(1)
$0.75^{\dagger}$	$I-S$	0.2880(8)	0.3290(8)	1.85
$0.75^{\ddagger}$	$I-S$	0.2873(8)	0.3288(9)	1.838(1)
$0.50^{\dagger}$	$I-S$	0.2376(13)	0.3087(13)	0.24
$0.50^{\ddagger}$	$I-S$	0.2345(16)	0.3076(12)	0.221(1)

A summary of the thermodynamic properties at the fluid–solid transition is given in Table IV.

The simulations in the high density region reported above provided no indication of a transition to a SmB liquid as the solid phase was expanded. For systems of soft parallel spherocylinders, however, simulations give evidence of a crystal-to-SmB transition that involves a significant volume change at the transition.[38,39] For the GB system we could not detect any density or enthalpy discontinuity on the equation of state. Although this transition is expected to be first order on the basis of symmetry arguments,[20,21] it could be very weak for GB systems and therefore difficult to observe. Stronger evidence of the absence (or presence) of an intermediate SmB phase may be obtained by measuring the in-layer pair distribution function $g_{\perp}(r_{\perp})$. This function measures positional correlations of the molecules within each single layer and so should allow to distinguish between a smectic phase [expected in-plane liquidlike behavior with no long range structure in $g_{\perp}(r_{\perp})$] and a true crystal phase. In order to get the behavior of $g_{\perp}(r_{\perp})$ at longer distances, this function was evaluated for substantially larger systems with $N=3150$ (six layers, each layer consisting of 525 molecules). $g_{\perp}(r_{\perp})$ was obtained along the solid branch of the isotherm $T=0.95$, expanding the system from $P=25.0$ in small pressure steps up to a pressure at which the system melted into the nematic phase. Again, no indications were found of any additional transition implying two-dimensional melting of crystal layers. As the crystal phase was expanded, $g_{\perp}(r_{\perp})$ exhibited considerable structure, with well-resolved peaks, the only observable effect being a slight broadening of the peaks and a decrease in the intensity of the first few peaks. Figure 4 illustrates $g_{\perp}(r_{\perp})$ for selected state points. At all pressures, the behavior of $g_{\perp}(r_{\perp})$ indicated clear crystalline order. The results presented here seem to confirm that the high-density SmB phase reported in previous studies for the GB fluid is in fact a molecular solid and is not a smectic liquid crystal phase.

In order to calculate the complete melting curve for temperatures $T<1.25$ we used GD integration. In principle, the implementation of the method requires knowledge of one single point on the coexistence curve as the initial starting point. Obviously, the coexistence properties will be subject to errors due (among other factors) to the finite integration step size used for the numerical integration of Eq. (8). These errors are expected to become larger as the integration proceeds, and may be particularly significant if the temperature range under investigation is wide. Thus, in order to minimize these propagation-of-error effects, we decided to use different starting points (particularly, those points obtained from the free energy calculations reported above) to cover different temperature ranges (see Table III).

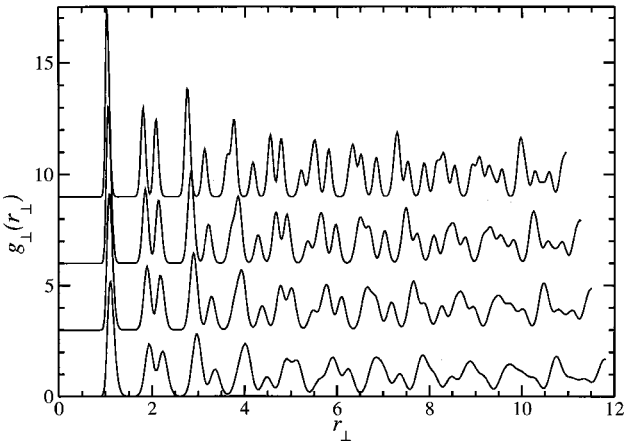

FIG. 4. Two-dimensional in-plane positional correlation function $g_{\perp}(r_{\perp})$ as obtained from constant pressure MC simulation for systems of 3150 GB particles at $T=0.95$ and different pressure values P. Each curve corresponds, from top to bottom, to $P=20$, 12, 8, and 5. The zero of $g_{\perp}(r_{\perp})$ has been shifted on the vertical scale for clarity.

The first series was started at $T=1.25$ and the temperature was decreased up to $T=0.95$ using a temperature step of 0.02. The corresponding results in the temperature-density and pressure–temperature diagram are shown in Figs. 5 and 6, respectively. As expected, the fluid phase in coexistence with the solid phase was found to exhibit nematic behavior in this range of temperatures. The $N-S$ transition properties for the lowest temperature in this range ($T=0.95$) have been included in Table IV. According to the results included in

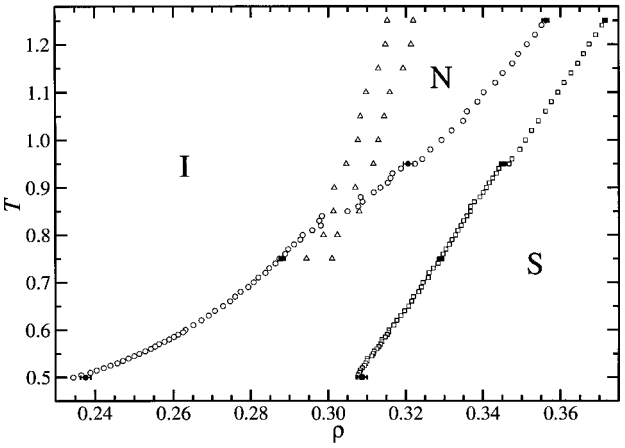

FIG. 5. Fluid–solid coexistence densities as a function of temperature T for the GB model. Circles represent fluid densities and squares represent solid densities. Filled symbols correspond to data obtained from free energy calculations and open symbols are data obtained from GD integration. Also included (open triangles) are the $I-N$ transition densities reported by de Miguel (Ref. 12).

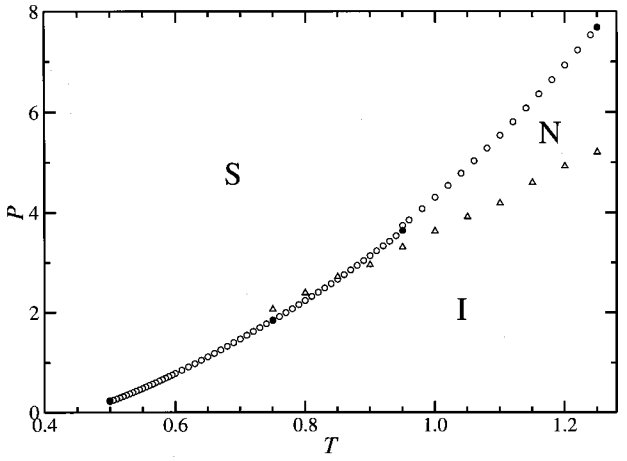

FIG. 6. Fluid–solid coexistence pressure P as a function of temperature T for the GB model as obtained from free energy calculation (filled circles) and GD integration (open circles). Also included (open triangles) are the $I-N$ transition pressures reported by de Miguel (Ref. 12). The $I-N-S$ triple point is located at $T_{INS}=0.85$ and $P_{INS}=2.70$.

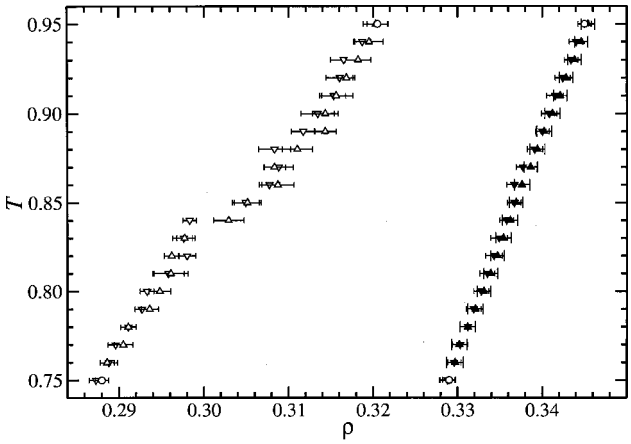

FIG. 7. Detail of the fluid–solid coexistence curve for the GB model in the neighborhood of the $I-N-S$ triple point. Down-triangles correspond to GD results on lowering the temperature from $T=0.95$ and up-triangles correspond to GD results on increasing the temperature from $T=0.75$. Open triangles represent fluid densities and filled triangles represent solid densities. Also included (open circles) are the fluid–solid densities obtained from free energy calculations.

this table, the transition properties obtained by GD integration compare reasonably well with those obtained by free energy calculations.

A second series of GD integration was designed to trace out the fluid–solid coexistence curve for temperatures $0.75 \leqslant T \leqslant 0.95$. We recall that, according to the free energy calculations reported above, the fluid phase in coexistence with the solid is nematic at $T=0.95$ and isotropic at $T=0.75$. Therefore, a nematic-to-isotropic transition is expected to take place in the fluid subsystem at some intermediate temperature. Starting from $T=0.95$, the temperature was reduced in steps of 0.01 up to $T=0.75$. The resulting coexistence densities and pressures are shown in Figs. 5 and 6. The corresponding values at the lowest temperature ($T=0.75$) have been included in Table IV and compared with those obtained from free energy calculations. Both procedures yield fully consistent results. Following the behavior of the nematic order parameter, the nematic-to-isotropic transition was observed to take place at $T\approx 0.85$. Also, as expected, this transition is accompanied by a small density jump, as can be observed in Fig. 5.

We should note that the use of the GD scheme requires the integration path be *reversible*. This may cast doubt on the reliability of the GD integration through the $N-I$ transition occurring at $T\approx 0.85$. We have attempted to check this issue by integrating up in temperature along the coexistence curve starting from $T=0.75$ in temperature steps of 0.01 up to $T=0.95$. Values of the coexistence densities at the fluid–solid transition resulting from integration up and down in this range of temperatures are shown in Fig. 7. In the heating series, the $I-N$ transition takes place at $T\approx 0.85$ and no significant hysteresis effects are observed at the transition. At the final temperature along this heating sequence ($T=0.95$), the GD integration yields a transition pressure $P_{NS}=3.669(1)$ which is in fairly good agreement with the value $P_{NS}=3.64$ obtained by thermodynamic integration and used as a starting point for the cooling sequence. From the results given in Fig. 7, we conclude that the GD integration path through the $I-N-S$ triple point is reversible. A similar conclusion was reported for the $I-N$ transition ocurring along the vapor–liquid line for other parametrizations of the GB model.[11] From the present results, the $I-N-S$ triple point is located at $T_{INS}=0.85$ and $P_{INS}=2.70$, the coexistence densities being $\rho_I=0.300$, $\rho_N=0.305$, and $\rho_S=0.337$, for the isotropic, nematic, and solid phases, respectively.

A new series of GD integration was started at $T=0.75$ from the corresponding coexistence data obtained previously by free energy calculations, and the integration was extended up to $T=0.50$. The integration proceeded in temperature steps of 0.01, although the step size was reduced to 0.005 for temperatures $T<0.60$. The fluid–solid transition properties obtained along this sequence are shown in Figs. 5 and 6 and the resulting pressure and densities at the lowest temperature ($T=0.50$) are presented in Table IV. The transition pressure obtained by GD integration ($P_{IS}=0.221$) is slightly lower than the value obtained from thermodynamic integration ($P_{IS}=0.24$).

The last GD integration series was initiated at $T=0.50$ and continued to lower temperatures. According to previous investigations, the GB fluid shows vapor–liquid separation in this region. In principle, integration of Eq. (8) may give rise to numerical unstabilities in this temperature range. This is because the transition pressure approaches zero as the temperature is lowered, and the right-hand side of Eq. (8) may grow quite large. The integration in this temperature range was then performed using Eq. (7) with an integration step of 0.0025. For temperatures $T<0.450$, the integration step was reduced to 0.001. Results are presented in Fig. 8. Results for the vapor–liquid equilibria as obtained from Gibbs ensemble simulations[11] are also shown in the figure. From these data, the (vapor–liquid) critical point is located at $T_c=0.473(10)$, $P_c=0.0134(9)$, the critical density being $\rho_c=0.100(14)$. According to Fig. 8, the GB model presents vapor–liquid separation over an unexpectedly narrow range of temperatures. Combining all the simulation data, the

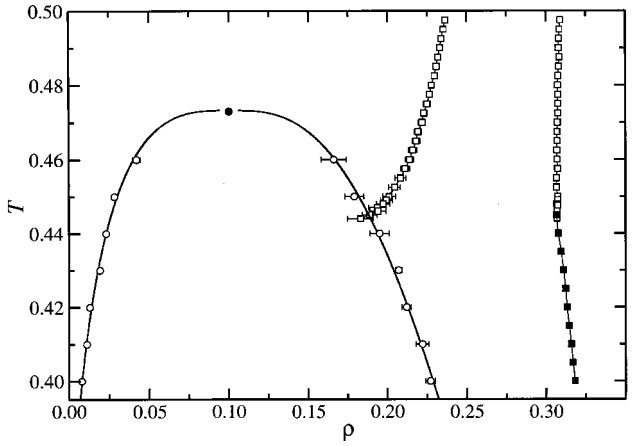

FIG. 8. Fluid–solid coexistence densities for the GB model at low temperatures as obtained from GD integration on lowering the temperature from $T=0.50$ (open squares). The filled squares represent solid densities obtained with zero-pressure *NPT* simulations. Open circles correspond to the vapor–liquid densities taken from Ref. 11 and the filled circle is the corresponding critical point. The $V-I-S$ triple point is located at $T_{VIS}=0.445$.

vapor–liquid–solid triple point is located at $T_{VIS}=0.445$, and $P_{VIS}=0.0072$, the coexistence densities being $\rho_V=0.026$, $\rho_I=0.189$, and $\rho_S=0.307$. As shown in Fig. 8, vapor–liquid equilibria is metastable for temperatures below T_{VIS}. Considering that the reduced vapor pressure of the solid along the sublimation line must be quite low, the solid density along the vapor–solid coexistence line was estimated from *NPT* simulations of the solid phase at zero pressure. Results from these simulations are included in Fig. 8.

IV. PHASE DIAGRAM

The resulting global phase diagram, derived from combining present and previous results, is given in Fig. 9 (temperature-density) and Fig. 10 (pressure-temperature).

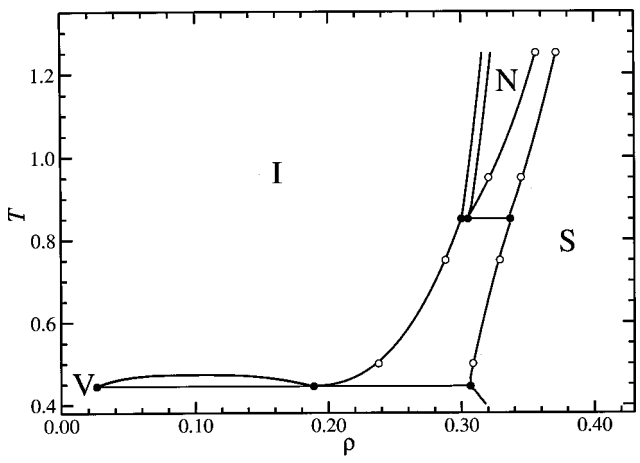

FIG. 9. Global temperature-density phase diagam of the GB model with anisotropy parameters $\kappa=3$ and $\kappa'=5$ as obtained from computer simulation showing the domain of thermodynamic stability of the vapor (V), isotropic (I), nematic (N), and solid (S) phases. The fluid-solid coexistence lines are the best fit to the GD data. Open circles are the fluid-solid coexistence densities obtained by free energy calculations. The $I-N$ coexistence lines are the best fit to the data reported in Ref. 12. Filled symbols correspond to the coexistence densities at the triple points.

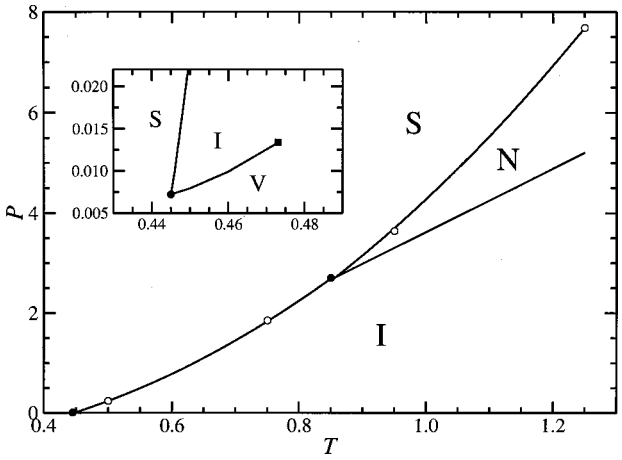

FIG. 10. Global pressure-temperature phase diagram of the GB model with anisotropy parameters $\kappa=3$ and $\kappa'=5$ as obtained from computer simulation showing the domain of thermodynamic stability of the vapor (V), isotropic (I), nematic (N), and solid (S) phases. The fluid–solid coexistence lines are the best fit to the GD data. Open circles are the fluid–solid coexistence densities obtained by free energy calculations. The $I-N$ coexistence line is the best fit to the data reported in Ref. 12. Filled circles correspond to the triple points and the filled square is the (isotropic) liquid–vapor critical point.

For temperatures $T<1.25$, the $I-N$ transition is weakly first order and characterized by a relative volume change $\approx 2\%$, which is rather insensitive to changes in temperature. The nematic phase is thermodynamically stable for temperature above $T_{INS}=0.85$. Although nematic behavior has been reported at lower temperatures,[12] for $T<T_{INS}$ the $I-N$ transition is pre-empted by the isotropic-to-solid transition. At high density, the nematic freezes into a solid phase through a first-order transition characterized by a relative volume change that increases as the temperature is lowered ($\approx 4\%$ at $T=1.25$ and $\approx 10\%$ at T_{INS}). The orientational order parameter of the solid phase at freezing is nearly constant and takes a value $S\approx 0.935$.

For temperatures $T<T_{INS}$, the solid phase melts directly into the isotropic fluid phase, the transition becoming increasingly stronger as the temperature is lowered. Below a critical point ($T_c=0.473$) (isotropic) liquid–vapor separation occurs. The vapor–isotropic–solid triple point is located at $T_{VIS}=0.445$. The fluid–solid transition is characterized by a significantly large relative density change at the transition, which is of about 47% at T_{VIS}. This is to be compared with the corresponding values of $\approx 12\%$ for the Lennard-Jones system[40] and $\approx 7\%$ for a two-center Lennard-Jones system[41] at the triple point. The large stability of the GB solid at low temperatures seems to be closely related to the strong attractive side-by-side molecular interactions. The orientational order of the solid phase at melting is observed to increase smoothly as T is lowered, with $S=0.947$ at T_{VIS}.

The $I-N$ transition line in the $P-T$ phase diagram (see Fig. 10) is quite straight over the range of temperatures considered here, with a slope $(dP/dT)_{IN}=6.34\pm 0.10$ (in reduced units), whereas the corresponding fluid–solid line shows a slight curvature towards the pressure axis with a slope $(dP/dT)_{FS}=9.17\pm 0.17$ at T_{INS}.

No evidence of smecticlike ordering has been found at

any of the temperatures investigated in this work. The present results suggest (1) the GB model does not exhibit SmB phase (at least, for this combination of parameters); and (2) the high-density phase, designated SmB in previous simulation studies,[6,9,12] corresponds to a crystal phase. As this phase resulted from *compressing* a translationally disordered fluid (at constant volume or at constant pressure) the crystalline order was incomplete. Therefore, it seems that the strong lateral attractive interactions present in the model tend to stabilize a layered structure, although the structure is crystalline.

ACKNOWLEDGMENTS

This work was financed by the Spanish DGI (Dirección General de Investigación) under Projects Nos. BFM2001-1420-C02-02 and BFM2001-1420-C02-01.

[1] *Structure of Liquid Crystals*, edited by P. S. Pershan (World Scientific, New York, 1988).
[2] P. G. de Gennes and J. Prost, *The Physics of Liquid Crystals*, 2nd ed. (Clarendon, Oxford, 1993).
[3] *Physical Properties of Liquid Crystals*, edited by D. Demus *et al.* (Wiley-VCH, New York, 1999).
[4] See, for example, M. P. Allen, in *Advances in the Computer Simulations of Liquid Crystals*, edited by P. Pasini and C. Zannoni (Kluwer, Dordrecht, 2000).
[5] J. G. Gay and B. J. Berne, J. Chem. Phys. **74**, 3316 (1981).
[6] G. R. Luckhurst, R. A. Stephens, and R. W. Phippen, Liq. Cryst. **8**, 451 (1990).
[7] E. de Miguel, L. F. Rull, M. K. Chalam, and K. E. Gubbins, Mol. Phys. **71**, 1223 (1990).
[8] E. de Miguel, L. F. Rull, M. K. Chalam, K. E. Gubbins, and F. van Swol, Mol. Phys. **72**, 593 (1991).
[9] E. de Miguel, L. F. Rull, M. K. Chalam, and K. E. Gubbins, Mol. Phys. **74**, 405 (1991).
[10] R. Hashim, G. R. Luckhurst, and S. Romano, J. Chem. Soc., Faraday Trans. **91**, 2141 (1995).
[11] E. de Miguel, E. Martín del Río, J. T. Brown, and M. P. Allen, J. Chem. Phys. **105**, 4234 (1996).
[12] E. de Miguel, Mol. Phys. **100**, 2449 (2002).
[13] E. Velasco, A. M. Somoza, and L. Mederos, J. Chem. Phys. **102**, 8107 (1995).
[14] E. Velasco and L. Mederos, J. Chem. Phys. **109**, 2361 (1998).
[15] G. R. Luckhurst and P. S. J. Simmonds, Mol. Phys. **80**, 233 (1993).
[16] M. P. Allen, J. T. Brown, and M. A. Warren, J. Phys.: Condens. Matter **8**, 9433 (1996).
[17] J. T. Brown, M. P. Allen, E. Martín del Río, and E. de Miguel, Phys. Rev. E **57**, 6685 (1998).
[18] M. A. Bates and G. R. Luckhurst, J. Chem. Phys. **110**, 7087 (1999).
[19] J. W. Goodby and G. W. Gray, in *Physical Properties of Liquid Crystals*, edited by D. Demus *et al.* (Wiley-VCH, New York, 1999), Chap. 2.
[20] C. C. Huang and T. Stoebe, Adv. Phys. **42**, 343 (1993).
[21] K. J. Strandburg, Rev. Mod. Phys. **60**, 161 (1988).
[22] R. J. Birgenau and J. D. Litster, J. Phys. (Paris) **39**, L399 (1978).
[23] B. I. Halperin and D. R. Nelson, Phys. Rev. Lett. **41**, 121 (1978).
[24] R. Pindak, D. E. Moncton, S. C. Davey, and J. W. Goodby, Phys. Rev. Lett. **46**, 1135 (1981).
[25] D. E. Moncton and R. Pindak, Phys. Rev. Lett. **43**, 701 (1979).
[26] C. Zannoni, in *The Molecular Physics of Liquid Crystals*, edited by G. R. Luckhurst and G. W. Gray (Academic, New York, 1979).
[27] S. Yashonath and C. N. R. Rao, Mol. Phys. **54**, 245 (1985).
[28] M. Parrinello and A. Rahman, Phys. Rev. Lett. **45**, 1196 (1980).
[29] D. Frenkel and A. J. C. Ladd, J. Chem. Phys. **81**, 3188 (1984).
[30] D. Frenkel and B. M. Mulder, Mol. Phys. **55**, 1171 (1985).
[31] D. Frenkel and B. Smit, *Understanding Molecular Simulation* (Academic, New York, 1996).
[32] C. Vega and P. A. Monson, J. Chem. Phys. **102**, 1361 (1995).
[33] N. Lu, C. D. Barnes, and D. A. Kofke, Fluid Phase Equilib. **194–197**, 219 (2002).
[34] D. A. Kofke, Mol. Phys. **78**, 1331 (1993).
[35] D. A. Kofke, J. Chem. Phys. **98**, 4149 (1993).
[36] P. J. Camp, C. P. Mason, M. P. Allen, A. A. Khare, and D. A. Kofke, J. Chem. Phys. **105**, 2837 (1996).
[37] F. J. Vesely, *Computational Physics* (Plenum, New York, 1994).
[38] K. M. Aoki and F. Yonezawa, Phys. Rev. Lett. **69**, 2780 (1992).
[39] K. M. Aoki and F. Yonezawa, Phys. Rev. A **46**, 6541 (1992).
[40] R. Agrawal and D. A. Kofke, Mol. Phys. **85**, 43 (1995).
[41] M. Lísal and V. Vacek, Mol. Simul. **19**, 43 (1997).